Spectroscopic and Density Functional Theory Studies of 1,10-Phenanthroline, Its Radical Anion, and $[Cu(Phen)(PPh_3)_2]^+$

Sarah L. Howell and Keith C. Gordon*

MacDiarmid Institute for Advanced Materials and Nanotechnology, Department of Chemistry, University of Otago, Union Place, Dunedin, New Zealand

Received: September 30, 2003

The vibrational spectra (Raman and IR) of 1,10-phenanthroline (phen), its perdeuterated analogue (d_8-1,10-phenanthroline, d_8-phen), and the copper(I) complexes $[Cu(phen)(PPh_3)_2]^+$ and $[Cu(d_8\text{-phen})(PPh_3)_2]^+$ have been measured. These spectra may be modeled using DFT calculations (B3LYP/6-31G(d)). The calculated structure compares favorably with crystallographic data. The time-resolved resonance Raman spectra of the copper(I) complexes were used to provide spectral signatures of $phen^{\bullet -}$ and d_8-$phen^{\bullet -}$. Geometries and vibrational spectra of the radical anions may be calculated in two ways: first as $phen^{\bullet -}$, which has been previously shown to be a $^2B_1$ state. Calculations with B3LYP require the 6-311+G(d,p) basis set in order to predict this state correctly for the radical anion, rather than the close-lying $^2A_2$ state, therefore giving a reasonable prediction of the geometry and spectra. Second, using $[Cu(phen^{\bullet -})(PH_3)_2]$ it is possible to model the radical anion at the B3LYP/6-31G(d) level because the metal center stabilizes the b_1 singly occupied ligand MO. The calculated spectra of $[Cu(phen^{\bullet -})(PH_3)_2]$ and its perdeuterated analogue compare favorably with experimental data for the excited state of the complexes.

Introduction

Polypyridyl complexes, such as those containing 1,10-phenanthroline (phen), have been studied for decades. Interest in these complexes arose because of their uses in areas such as nanotechnology,[1] photocatalysis,[2] and solar cell devices.[3] The key excited state in the utility of metal polypyridyl complexes in these areas is the metal-to-ligand charge transfer (MLCT) excited state, in which the metal is formally oxidized and one of the ligands in the complex is formally reduced to a radical anion.[4] We are interested in establishing the structural changes that occur in metal complexes with polypyridyl ligands upon photoexcitation. As a starting point to this, we have investigated the phen ligand and its radical anion using density functional theory (DFT) calculations to model the measured vibrational spectra.

The vibrational spectra of phen have been studied since 1974.[5] More recently, Thornton and Watkins studied the vibrational spectra of phen and its perdeuterated analogue, d_8-phen.[6] Muniz-Miranda carried out normal-mode calculations on phen in order to interpret the surface-enhanced Raman spectrum of phen adsorbed on silver sols.[7] This study uses DFT calculations to carry out a normal coordinate analysis of phen, d_8-phen, and their radical anions and consider the effects of complexation on these modes.

The resonance Raman spectroscopy of $[Ru(phen)_3]^{2+}$ and its MLCT excited state provided some initial findings as to the vibrational spectra of phen and its radical anion.[8] The resonance Raman effect resulted in the scattering enhancement of the phen modes through the MLCT transition. Using pulsed laser excitation in a single-color pump−probe experiment,[9] the resonance Raman scattering of the excited state was measured. The observed excited-state spectrum for $[Ru(phen)_3]^{2+}$ showed some differences from the ground-state spectrum. However, such a complex has a number of active chromophores in the MLCT excited state, and both phen and $phen^{\bullet -}$ features were assigned. A later study used resonance Raman spectroscopy to probe alkali metal salts of $phen^{\bullet -}$ and provided a detailed spectral survey of the radical anion species.[10] The Raman spectrum of $phen^{\bullet -}$ has proved to be difficult to measure; this is attributed, in part, to its weak Raman scattering ability compared to that of the well-studied radical anion of 2,2′-bipyridine (bpy).[11] Schoonover et al. have studied the resonance Raman (RR) spectra of $[Ru(phen)_3]^{2+}$, its reduced product, and the MLCT excited state, $[Ru(phen)_3]^{2+}*$.[11] Their data demonstrate very clearly the difficulties of observing $phen^{\bullet -}$ bands in a complex such as $[Ru(phen)_3]^{2+}$ and provide assignments of the phen and $phen^{\bullet -}$ bands present in $[Ru(phen)_3]^{2+}*$.

Computational modeling with a variety of basis sets has been used to predict some of the properties of ligands and metal complexes thereof. These include geometry,[12] MO types,[13] and vibrational spectra.[14] Recent work has used DFT calculations to examine large polypyridyl ligands such as dipyrido[3,2-a:2′,3′-c]phenazine (dppz) and also calculated the spectra of isotopomers of this ligand to aid spectral interpretation.[15] A number of recent studies have focused on calculating properties of metal polypyridyl complexes. For example, Rillema et al. in a study of 10 ruthenium(II) diimine complexes have shown that the spectroscopic and electrochemical properties may be correlated to the HOMO−LUMO energies derived from geometry calculations using B3LYP/3-21G* and B3LYP/3-21G**.[16] A series of papers by Zheng et al. have shown that, using B3LYP/LANL2DZ, it is possible to relate geometry and MO calculations to the electronic properties of complexes such as $[Ru(phen)_3]^{2+}$ and its substituted analogues.[13] The first example of the use of DFT methods to predict the vibrational spectra of the ground and excited states of a metal polypyridyl complex, $[Re(CO)_3$-

* Corresponding author. E-mail: kgordon@alkali.otago.ac.nz.

10.1021/jp031108e CCC: $27.50
Published on Web 03/09/2004

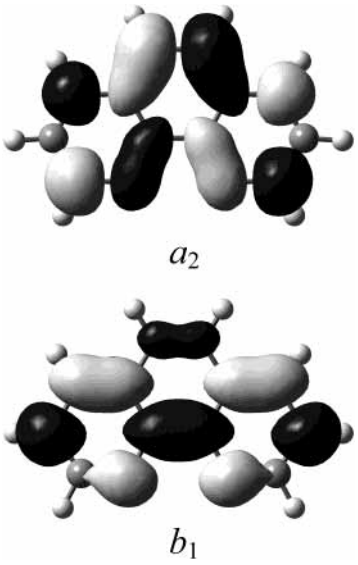

Figure 1. LUMO (b_1 symmetry) and LUMO+1 (a_2 symmetry) of phen.

(bpy)(4-ethylpyridine)]$^+$, has been reported recently.[17] Few studies have attempted to use computational techniques to model the structural differences attendant upon the reduction of a ligand. Castella-Ventura et al. carried out ab initio calculations on 4,4′-bipyridine.[18] They examined the force constants, vibrational frequencies, and potential energy distributions as well as the structure of 4,4′-bipyridine, its radical anion, and its dihydro dication radical. They found that whereas the bpy derivative has a twisted conformation with respect to the two pyridine rings the charged species have an overall planar conformation. Vibrational frequencies were compared to measured Raman spectra, and the effect of deuteration was measured experimentally and compared to calculated effects. Similar studies by McCusker et al. on the ligand 4-arylpyridine[19] were related to the behavior of the Ru complexes with phenyl substituents on the 2,2′-bipyridyl ligand.

This work investigates the structural changes that occur upon the reduction of phen using DFT calculations and vibrational spectroscopy. The electronic structure of phen$^{\bullet -}$ has proven challenging to determine and was quite uncertain in nature until recently.[20] Two types of unoccupied molecular orbitals are close in energy—the a_2 and b_1 molecular orbitals (Figure 1)—and either may be the singly occupied molecular orbital (SOMO) in the radical species. A number of elegant studies using EPR and ENDOR have proven that phen$^{\bullet -}$ is a $^2B_1$ state[20] and that the substitution of phen can lead to a $^2A_2$ radical anion state.[21] Attempts to model the radical anion have also proven challenging, where DFT calculations require large basis sets with the inclusion of polarization functions.[22] There have been, to our knowledge, no attempts to model the vibrational spectra of phen$^{\bullet -}$ using ab initio calculations. The neutral species can be studied using infrared (IR) and Raman spectroscopy. d_8-Phen is also studied to aid in spectral interpretation. A comparison of these measured spectra to vibrational spectra of phen and d_8-phen predicted by DFT calculations enables a normal coordinate analysis of phen to be carried out. Vibrational spectra of [Cu(phen)(PPh$_3$)$_2$]$^+$ are collected and compared to both the vibrational spectra of phen to empirically determine the effect that the metal center has on the vibrational modes and the spectra calculated for [Cu(phen)(PH$_3$)$_2$]$^+$. The use of the PH$_3$ ancillary ligand over PPh$_3$ greatly reduces the computational difficulty and has little effect on the structure of the complex with respect to the phen section of the complex. Time-resolved resonance Raman (TR^3) spectroscopy of [Cu(phen)(PPh$_3$)$_2$]$^+$ is utilized to probe the vibrational modes that are characteristic of phen$^{\bullet -}$ as an MLCT excited state is formed. This strategy has a number of advantages for the study of phen$^{\bullet -}$. First, the MLCT excited state of [Cu(phen)(PPh$_3$)$_2$]$^+$ should not be as complex as that from a [Ru(phen)$_3$]$^{2+}$ species in which a phen → Ru(III) transition can occur. The primary scatterer, at the excitation wavelength used, from [Cu(phen)(PPh$_3$)$_2$]$^+$* should be phen$^{\bullet -}$. Second, using the d_8-phen complex provides an additional method of observing and analyzing phen$^{\bullet -}$ modes because some of these will be selectively shifted through substitution. Finally, it has been suggested that the chemical reduction of phen can result in mixtures of phen$^{\bullet -}$ and phen^{2-}, which can clearly lead to complications in spectral interpretation.[11] This problem does not occur when using the MLCT excited state of [Cu(phen)(PPh$_3$)$_2$]$^+$. The Raman spectrum of the MLCT state is modeled using the reduced complex [Cu(phen$^{\bullet -}$)(PH$_3$)$_2$] and its deuterated analogue [Cu(d_8-phen$^{\bullet -}$)(PH$_3$)$_2$] in calculations and in comparing these to the experimental data for the corresponding PPh$_3$ complexes.

Experimental Section

Syntheses. *Materials.* All reagents were purchased commercially and used without further purification, except for PPh$_3$, which was recrystallized from ethanol before use.

d_8-Phen was prepared by a variation of the method developed by Junk et al.[23] [Cu(PPh$_3$)$_4$]BF$_4$, [Cu(phen)(PPh$_3$)$_2$]BF$_4$, and [Cu(d_8-phen)(PPh$_3$)$_2$]BF$_4$ were prepared by the method described by McMillin et al.[24]

Perdeuterated 1,10-Phenantholine (d_8-Phen). Yield: 90%. ^{2}H NMR (CHCl$_3$, 500 MHz): δ 9.18 (s, 2D), 8.23 (s, 2D), 7.77 (s, 2D), 7.62 (s, 2D). ^{13}C NMR (CDCl$_3$, 300 MHz): δ 149.9 (t, J = 110 Hz), 146.3 (s), 135.5 (t, J = 99 Hz), 128.5 (s), 126.0 (t, J = 97 Hz), 122.5 (t, J = 95 Hz). MS (ES) m/z: 189 (MH$^+$). Found: C, 71.14; H, 4.89; N, 14.24. Calcd for $C_{12}D_8N_2 \cdot (H_2O)_{0.8}$: C, 71.15; H, 4.78; N, 13.83.[25]

[Cu(phen)(PPh$_3$)$_2$]BF$_4$. Yield: 53%. ^{1}H NMR (CDCl$_3$, 300 MHz): δ 8.71 (s, 2H), 8.55 (d, 2H, J = 7.2 Hz), 8.04 (s, 2H), 7.77 (t, 2H, J = 7.8 Hz), 7.34−7.29 (m, 6H), 7.18−7.06 (m, 24H). ^{13}C NMR (CDCl$_3$, 300 MHz): δ 149.7, 143.8, 138.1, 133.2, 132.5, 130.3, 129.9, 129.0, 127.7, 125.3. MS (ES) m/z: 767 (M − BF$_4$). Found: C, 67.12; H, 4.50; N, 3.61. Calcd for $CuC_{48}H_{38}N_2P_2BF_4$: C, 67.41; H, 4.47; N, 3.28%.

[Cu(d_8-phen)(PPh$_3$)$_2$]BF$_4$. Yield: 37%. ^{2}H NMR (CHCl$_3$, 500 MHz): δ 8.56 (s, 4D), 8.04 (s, 2D), 7.73 (s, 2D). ^{13}C NMR (CHCl$_3$, 500 MHz): δ 149.0, 143.2, 137.7, 133.0, 132.0, 132.3, 129.7, 128.9, 127.1, 124.7. MS (ES) m/z: 775 (M-BF$_4$). Found: C, 66.57; H, 4.34; N, 3.45. Calcd for $CuC_{48}H_{30}D_8N_2P_2BF_4$: C, 66.79; H, 4.44; N, 3.25.

Physical Measurements. *Synthetic Analysis.* ^{1}H NMR and ^{13}C NMR spectra were recorded at 25 °C using either a Varian 300- or 500-MHz NMR spectrometer. ^{2}H NMR spectra were recorded at 25 °C on a Varian 500-MHz NMR spectrometer. Chemical shifts are given relative to residual solvent peaks. Microanalyses were performed at the Campbell Microanalysis Laboratory at the University of Otago. Mass spectrometry measurements were obtained from a Micromass LCT instrument for electrospray (ES) measurements.

IR Spectroscopy. FT-IR spectra were collected, using a Perkin-Elmer Spectrum BX FT-IR system with Spectrum v. 2.00 software, of potassium bromide (KBr) disks of phen, d_8-phen, and their copper complexes. Spectra were measured using 64 scans. Band positions are reproducible within 1−2 cm^{-1}.

TABLE 1: Calculated and Experimental Structural Parameters for Phen, Phen$^{\bullet -}$, and Copper(I) Complexes

	phen		$[Cu(phen)(PH_3)_2]^+$	$[Cu(phen)(PPh_3)_2]^+$	phen$^{\bullet -}$ calcd	$[Cu(phen^{\bullet -})(PH_3)_2]$
	calcd	exptl[a]	B3LYP/6-31G(d)	exptl[b]	B3LYP/6-311+G(d,p)	B3LYP/6-31G(d)
bond/Å						
N1−C2	1.32	1.32 ± 0.01	1.33	1.33 ± 0.01	1.32	1.35
N1−C12	1.35	1.34 ± 0.02	1.36	1.36 ± 0.01	1.39	1.40
C2−C3	1.41	1.39 ± 0.04	1.40	1.39 ± 0.02	1.40	1.39
C3−C4	1.38	1.35 ± 0.03	1.38	1.37 ± 0.02	1.41	1.41
C4−C13	1.41	1.39 ± 0.02	1.41	1.41 ± 0.01	1.39	1.39
C5−C6	1.36	1.35 ± 0.01	1.36	1.35 ± 0.02	1.36	1.36
C5−C13	1.43	1.42 ± 0.02	1.44	1.43 ± 0.01	1.44	1.44
C11−C12	1.46	1.44 ± 0.01	1.44	1.44± 0.01	1.40	1.41
C12−C13	1.42	1.41 ± 0.03	1.42	1.40 ± 0.01	1.45	1.43
N1−Cu			2.02	2.07 ± 0.01		1.99
angle/deg						
N1−C2−C3	124	123 ± 3	123	123	126	124
N1−C12−C11	119	118 ± 1	118	117	120	118
C2−N1−C12	118	118 ± 2	118	118	118	117
C2−C3−C4	118	118 ± 2	119	120	117	119
C3−C4−C13	119	121 ± 2	119	119	120	119
C4−C13−C12	118	117 ± 2	117	117	119	119
C5−C13−C12	120	120 ± 2	119	119	119	118
C6−C5−C13	121	121 ± 3	121	121	121	122
N1−Cu−N10			84	81		86

[a] Reference 32. [b] Reference 33.

Raman Spectroscopy. FT-Raman spectra were collected on powder samples using a Brucker IFS-55 FT-interferometer bench equipped with an FRA/106 Raman accessory and utilizing OPUS (version 4.0) software. An Nd:YAG laser with 1064-nm excitation wavelength was used. An InGaAs diode (D424) operating at room temperature was used to detect Raman photons. Spectra were measured using 16 scans at a power of 100 mW and a resolution of 4 cm^{-1} for phen and d_8-phen and with 200 scans for the copper complexes.

A continuous-wave Innova I-302 krypton-ion laser (Coherent, Inc.) was used to generate resonance Raman (RR) scattering. Bandpass filters removed the Kr^+ plasma emission lines from the laser output. Typically, the laser output was adjusted to give 60 mW at the sample. The incident beam and the collection lens were arranged in a 135° backscattering geometry to reduce Raman intensity reduction by self-absorption.[26] An aperture-matched lens was used to focus scattered light through a narrow band line-rejection (notch) filter (Kaiser Optical Systems) and a quartz wedge (Spex) and onto the 100-μm entrance slit of a spectrograph (Acton Research SpectraPro 500i). The collected light was dispersed in the horizontal plane by a 1200 grooves/mm ruled diffraction grating (blaze wavelength 500 nm) and detected by a liquid-nitrogen-cooled back-illuminated Spec-10: 100B CCD controlled by a ST-133 controller and WinSpec/32 (version 2.5.8.1) software (Roper Scientific, Princeton Instruments).

The frequency-tripled output from a Nd:YAG (Continuum Surelite I-10) pulsed laser (5−7-ns pulse width, operating at 10 Hz) was used for the TR^3 experiments. Typically, a 355-nm, 1.1−3.6-mJ pump pulse was used. The beam diameter at the sample was ∼300 μm.

Wavenumber calibration was performed using Raman bands from a 1:1 v/v acetonitrile/toluene sample.[27,28] Peak positions were reproducible to within 1−2 cm^{-1}. Spectra were obtained with a resolution of 5 cm^{-1}.

Freshly prepared samples were held in a spinning NMR tube. The concentrations used were approximately 10 mmol dm^{-3} in CH_2Cl_2 for $[Cu(phen)(PPh_3)_2]^+$ and $[Cu(d_8\text{-phen})(PPh_3)_2]^+$ and ca. 15 mmol dm^{-3} for $[Cu(PPh_3)_4]^+$ for RR and TR^3 measurements.

Spectroscopic-grade solvents were used for all spectroscopic measurements.

Spectral data was analyzed using Galactic Industries GRAMS/32 AI software.

Calculations. The geometry and vibrational frequencies along with their IR and Raman intensities were calculated using DFT calculations (B3LYP functional) with basis sets 6-31G(d) and 6-311+G (d,p). These were implemented with the Gaussian 98W[29] and Gaussian 03W[30] program packages. The visualization of the vibrational modes was provided by the Molden package[31] and GaussViewW (Gaussian Inc.).

Results and Discussion

Neutral Ligand: Spectra and Calculations. The calculated structural parameters of phen are shown in Table 1, along with the previously published X-ray crystal structures of 1,10-phenanthroline monohydrate [32] and $[Cu(phen)(PPh_3)_2]^+$.[33] The calculated structure of phen (B3LYP/6−31(d)) has an average C−C bond length of 1.41 Å. The C−N bonds are shorter at 1.32 and 1.35 Å. This is in close agreement with the observed structural data of phen (within 0.01 Å). The calculated bond angles are also within experimental uncertainty. The geometry calculated with B3LYP/6-311+G(d,p) is very similar to that calculated with the 6-31G(d) basis set. The coordination of phen to the $\{Cu(PPh_3)_2\}^+$ moiety was found to buckle the ligand slightly. Coordinating nitrogens N1 and N10 lie below (0.145 Å) and above (0.057 Å) the least-squares plane, respectively. This did not largely perturb the bond lengths and angles of phen. To simplify the calculations on the copper complex and because it is the phen geometry and modes that are primarily of interest, $[Cu(phen)(PH_3)_2]^+$ was modeled instead of $[Cu(phen)(PPh_3)_2]^+$. The calculation is in agreement with the observation that there is little structural change to phen upon coordination to a Cu(I) center. This is not surprising because phen is a very rigid ligand. The N1−Cu bond is predicted to be shorter, at 2.02 Å, than the observed bond length of 2.07 Å. The N1−Cu−N10 bond angle has been overestimated by 3°, at 84°. However, these are not large differences for metal−ligand bonds and angles,[34] and the geometry of phen in the complex has been well predicted. For

TABLE 2: Calculated and Experimental Vibrational Spectral Data of Phen, d_8-Phen, and Their Copper(I) Complexes

		phen				[Cu(phen)$(PH_3)_2]^+$		[Cu(phen)$(PPh_3)_2]^+$	d_8-phen				[Cu(d_8-phen)$(PH_3)_2]^+$		[Cu(d_8-phen)$(PPh_3)_2]^+$	
		B3LYP/6-31G(d)		exptl		B3LYP/6-31G(d)		exptl[c]	B3LYP/6-31G(d)		exptl		B3LYP/6-31G(d)		exptl[c]	
ν[a]		ν/cm^{-1}	(IR, R Int)[b]	ν/cm^{-1}	(IR, R Int)	ν/cm^{-1}	(IR, R Int)	ν/cm^{-1}	ν/cm^{-1}	(IR, R Int)	ν/cm^{-1}	(IR, R Int)	ν/cm^{-1}	(IR, R Int)	ν/cm^{-1}	%PED[d]
30	b_2	1029	(3, 1)	1026	(2, 0)	1024	(0, 0)	1024	1003	(15, 0)	1007	(4, 0)	1001	(0, 0)		A(10), C(90)
31	a_1	1034	(1, 16)	1037	(8, 18)	1053	(0, 37)	1053	848	(5, 15)	859	(0, 13)	866	(0, 17)	872	A(10), C(70)
32	b_2	1069	(7, 0)	1079	(11, 0)	1081	(0, 0)		848	(2, 0)	855	(15, 0)				A(20), C (60)
33	a_1	1092	(26, 5)	1091	(27, 0)	1097	(3, 8)	1098	876	(34, 4)	884	(35, 4)	885	(3, 1)	888	A(20), C(40)
34	b_2	1134	(19, 1)	1137	(18, 2)	1141	(4, 3)	1142	837	(6, 3)	844	(9, 5)	849	(3, 2)	858	C(20)
35	a_1	1140	(3, 1)	1141	(19, 0)	1150	(0, 4)		830	(2, 2)	836	(9, 3)	834	(0, 3)	838	A(10), B(10), C(20)
36	a_1	1192	(0, 11)	1188	(0, 3)	1203	(0, 8)	1187	1121	(0, 17)	1119	(4, 12)	1128	(0, 23)	1127	A(20), B(30), C(50)
37	a_1	1202	(0, 0)	1205	(2, 2)	1209	(2, 6)	1212					972	(0, 5)		A(40), B(10)
38	b_2	1219	(1, 2)	1218	(15, 2)	1220	(1, 0)	1223	1016	(0, 1)			1026	(1, 1)		A(20), B(30), C(20)
39	b_2	1268	(2, 3)	1270	(0, 4)	1257	(0, 0)		1026	(0, 2)	1032	(11, 0)	1012	(1, 1)	1036	A(10), B(10), C(40)
40	a_1	1291	(4, 26)	1296	(4, 34)	1307	(1, 35)	1299	1259	(3, 15)	1255	(0, 10)	1272	(2, 9)	1261	A(30), B(10), C(40)
41	b_2	1309	(1, 3)	1314	(0, 3)	1322	(0, 3)	1317	1302	(3, 6)	1295	(18, 5)	1316	(0, 1)	1309	A(50), C(50)
42	a_1	1349	(3, 19)	1346	(23, 11)	1339	(0, 27)	1342	1199	(2, 9)	1208	(0, 8)	1211	(0, 6)	1215	A(20), C(40)
43	a_1	1383	(0, 100)	1406	(20, 100)	1409	(2, 100)	1419	1321	(6, 46)	1332	(0, 12)				A(60), B(20), C(10)
44	b_2	1414	(0, 3)			1413	(15, 2)		1256	(39, 5)	1256	(44, 0)	1261	(4, 3)		A(10), B(20), C(10)
45	b_2	1421	(100, 1)	1421	(100, 16)	1422	(18, 1)	1426	1338	(35, 0)	1335	(71, 0)	1332	(12, 0)	1339	A(40), B(10), C(20)
46	a_1	1449	(3, 13)	1448	(9, 31)	1446	(1, 47)	1450	1402	(4, 100)	1414	(10, 100)	1413	(0, 100)	1423	A(20), B(10), C(30)
47	b_2	1499	(15, 1)	1492	(32, 0)	1495	(4, 1)	1495	1437	(27, 0)	1428	(44, 0)	1430	(7, 0)	1436	A(10), B(40), C(40)
48	a_1	1504	(80, 17)	1504	(51, 16)	1513	(10, 17)	1512	1465	(100, 15)	1464	(76, 22)	1472	(7, 16)	1469	A(20), B(10), C(50)
49	b_2	1557	(30, 7)	1562	(30, 7)	1577	(4, 28)	1574	1538	(88, 5)	1543	(100, 0)	1552	(4, 9)	1552	A(30), C(60)
50	a_1	1598	(23, 10)	1588	(31, 17)	1589	(2, 11)	1587	1566	(44, 12)	1552	(82, 12)	1552	(10, 11)		A(10), B(10), C(80)
51	b_2	1611	(17, 9)	1602	(0, 12)	1602	(1, 15)	1601	1586	(46, 11)	1579	(7, 14)	1577	(1, 16)		A(20), B(10), C(70)
52	a_1	1622	(19, 5)	1617	(19, 7)	1624	(8, 10)	1624	1592	(2, 7)	1591	(8, 9)	1596	(3, 6)		A(20), B(60), C(20)

[a] Mode numbers and symmetries are from the B3LYP/6-31G(d) calculation of phen. [b] IR and Raman intensities have been normalized such that the strongest band in the region of interest is given an intensity of 100. Raman intensities have been calculated using an excitation wavelength of 1064 nm. [c] Experimental IR and Raman intensites of the Cu(I) complexes have not been reported because many of the bands have an intensity contribution from PPh_3. [d] %PED is defined in Figure 2.

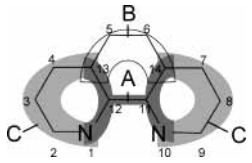

Figure 2. Numbering system for phen and %PEDs designated: (A) motion of atoms 1 and 10−14; (B) motion of atoms 5, 6, 13, and 14; (C) motion of atoms 1−4, 7−10, 13, and 14.

the experimental data, the bond lengths and angles are the same (within experimental uncertainty) for complexed and uncomplexed phen.

The optimized structures of phen and [Cu(phen)$(PH_3)_2]^+$ were used to calculate the vibrational frequencies and intensities. The calculated and measured vibrational data of phen, d_8-phen, [Cu(phen)$(PPh_3)_2]^+$, and [Cu(d_8-phen)$(PPh_3)_2]^+$ are presented in Table 2. The calculated Raman intensities are based on an excitation wavelength of 1064 nm.[35] Calculated frequencies have been scaled by a factor of 0.9796 for phen with the 6-31G(d) basis set, 0.9807 for phen with the 6-311+G(d,p) basis set, and 0.9695 for the copper complexes (with the 6-31G(d) basis set).[36] The calculation produced no imaginary frequencies, which is consistent with an energy minimum for the geometry used.[37]

Generally, the normal modes of vibration associated with the observed vibrational transitions involve the nuclei motions of many atoms in a molecule. The normal modes for phen can be described by the percentage potential energy distribution (%PED),[38] which has been parametrized into A, B, and C as depicted in Figure 2. These three parameters all describe the stretching and bending of the rings and do not consider the CH stretching and bending. The value assigned for A is the percentage contribution, to the normal mode, of the motion (stretching and bending) of the central part of the phen ligand. B is the motion of the remainder of the central ring not described by parameter A. The final parameter C describes the motion of the other two rings, again excluding the central region as defined by A. In the region discussed, there is no contribution to the %PED from out-of-plane modes. The changes in the modes of phen upon deuteration are tracked using available programs.[39]

In the region from 1000−1700 cm^{-1}, B3LYP/6-31G(d) predicts 23 vibrational modes for phen. Twenty-two of these modes are observed in the measured IR and Raman spectra. The only mode not observed is ν_{44}, which is predicted by the calculation to have no intensity in the IR spectrum and very little in the Raman spectrum. Of the 22 observed modes, the calculation predicts 17 to within 5 cm^{-1} and 4 to within 6−10 cm^{-1}. The remaining one is 23 cm^{-1} lower than the observed frequency (ν_{43}). It is of interest how the bands shift upon deuteration and whether these shifts can be accurately predicted by the calculation in order to test the robustness of the calculation and aid in spectral interpretation. The shifts observed for each mode upon deuteration are reproduced in the calculated spectra to within 13 cm^{-1}, with half of the frequency shifts within 5 cm^{-1}. The relative intensities of the bands for both phen and d_8-phen have also been well predicted.

The IR spectrum of phen shows 11 bands of moderate to strong intensity in the region from 1000−1700 cm^{-1}. The strongest band in this region is both observed at 1421 cm^{-1} and predicted at 1421 cm^{-1} (ν_{45}). Upon deuteration, this band shifts to 1335 cm^{-1}, predicted at 1338 cm^{-1}, and decreases slightly in relative intensity. This mode can be described as being mainly A in character as well as having contributions from B and C. ν_{34}, observed at 1137 cm^{-1} and predicted at 1134 cm^{-1}, shows a large shift in frequency upon deuteration. It is observed at 844 cm^{-1} in the IR spectrum of d_8-phen, predicted at 837 cm^{-1}. ν_{34} has a 20% contribution from C only, making it a predominantly CH motion, explaining the large shift upon deuteration. Conversely, a medium-intensity band at 1562 cm^{-1}, predicted at 1557 cm^{-1} (ν_{49}), shows a modest shift to 1543 cm^{-1} upon deuteration, predicted to shift to 1538 cm^{-1}. There is a significant increase in the observed and predicted intensities of this mode upon deuteration. This mode is described as being 30% A and 60% C, hence having a small CH motion contribution.

The FT-Raman spectrum of phen shows six bands of medium to weak intensity in the spectral range of interest. The most intense band in this region, significantly larger than any other band, is ν_{43} at 1406 cm^{-1}, predicted at 1383 cm^{-1}. Upon deuteration, this mode shifts down to 1332 cm^{-1}, predicted at 1321 cm^{-1}. Along with this moderate shift in frequency comes a substantial decrease in the intensity of the band, which is also predicted. ν_{43} can be described as being mainly A in character with contributions from both B and C. The second strongest band, at approximately one-third of the intensity of ν_{43}, is ν_{40}. This band is observed at 1296 cm^{-1}, predicted at 1291 cm^{-1}. In the FT-Raman spectrum of d_8-phen, this mode shifts to 1255 cm^{-1}, predicted at 1259 cm^{-1}. The %PED of ν_{40} is largely due to A and C. Another band of interest in the FT-Raman spectrum of phen is ν_{46}, a band of medium intensity observed at 1448 cm^{-1} and predicted at 1449 cm^{-1}. Upon deuteration, there is a large increase in intensity. This mode is predicted and observed to be the strongest band in the region. The band is now observed at 1414 cm^{-1}, predicted at 1402 cm^{-1}. ν_{46} can be described as mainly A and C in character.

Calculations on phen have also been carried out using B3LYP/6-311+G(d,p). The earlier part of this discussion has demonstrated that the 6-31G(d) basis set adequately predicts the structure and vibrational spectra of phen. The larger basis set makes no significant difference to the calculated vibrational spectra: frequencies are within 2 cm^{-1}, and there is little change to the relative intensities. However, the 6-311+G(d,p) basis set appears to be the smallest choice with the B3LYP method, which orders the molecular orbitals correctly in the radical anion. Because the LUMO and LUMO+1 lie at similar energies because of configuration interaction, this may lead to either being populated in the radical anion state. The HOMO, LUMO, and LUMO+1 have symmetries of b_1, b_1, and a_2, respectively, within the C_{2v} point group. Calculations with B3LYP/6-31G(d) predict a $^2A_2$ state rather than the $^2B_1$ state that phen$^{\bullet -}$ is, as demonstrated by EPR studies.[20] B3LYP/6-311+G(d,p) correctly predicts a $^2B_1$ state. Although Kaim et al.[22] showed that the 6-31G(d,p) basis set was sufficient with the Hartree−Fock method, B3LYP/6-31G(d,p) predicts a $^2A_2$ state for phen$^{\bullet -}$. The B3LYP/6-311+G(d,p) calculation correctly predicts a $^2B_1$ state, whereas calculations with the smaller basis sets 6-31G(d), 6-31G(d,p), 6-31+G(d), and 6-311G(d,p) predict the $^2A_2$ state for phen$^{\bullet -}$. Presumably, the success of the B3LYP/6-311+G(d,p) calculation is attributable to the basis set size used.

The bands in the vibrational spectra of the phen and d_8-phen complexes are correlated to the calculated phen and d_8-phen modes both empirically, by comparison to the respective vibrational spectra of the uncomplexed ligand, and by using available programs[39] to compare the calculated vibrational modes. It is expected that some modes will be affected by coordination to metal centers whereas others will not, depending on the nature of the mode. It is also expected that the effect observed with the phen modes should be replicated with the d_8-phen modes. This is seen for many, but not all, of the modes.

The geometries and vibrational spectra of the copper complexes have been calculated using B3LYP/6-31G(d). The presence of the Cu(I) center leads to a stabilization of the b_1 unoccupied molecular orbital (UMO). This stabilization reduces the configuration interaction between the close-lying UMOs. As a result of this, [Cu(phen$^{\bullet -}$)$(PH_3)_2$] is predicted to be a $^2B_1$ state, in agreement with experimental findings for complexes containing phen$^{\bullet -}$.[21,22]

The complexation of phen and d_8-phen with the Cu(I) center shifts the bands between −4 and +16 cm^{-1} (Table 2). The calculation predicts shifts of −14 to +26 cm^{-1}. Most bands were increased in energy for both phen and d_8-phen. ν_{31} showed the largest shifts in both the phen and d_8-phen cases—increases of 16 and 13 cm^{-1}, respectively, calculated to increase by 19 and 18 cm^{-1}. A couple of bands were unaffected by coordination, remaining at the same wavenumber (within 2-cm^{-1} shifts, which is within peak reproducibility) for both phen and d_8-phen: ν_{35} and ν_{50}. These modes were predicted to have shifts of up to 14 cm^{-1}. Many modes show very different shifts, upon coordination, from phen to d_8-phen. For example, ν_{42} decreases in energy by 4 cm^{-1} for phen (predicted to decrease by 10 cm^{-1}) but increases in energy by 7 cm^{-1} for d_8-phen (predicted to increase by 12 cm^{-1}). No obvious correlation between the effect of coordination of the $[Cu(I)(PPh_3)_2]^+$ moiety and the nature of the modes can be made. This is similar to the results found during studies by Thornton et al.[40] and Campos-Vallette et al.[41] Thorton et al. in a detailed study of a series of phen and d_8-phen complexes with a variety of metal centers found that the majority of bands shifted to higher frequency upon coordination but that there was no clear correlation between the effect of complexation and the nature of the modes. The study of Cu(I) and Cu(II) bis-phen complexes by Campos-Vallette et al. found that the observed IR bands of phen generally shifted to higher frequencies upon coordination to the copper centers.

Radical Anion: Spectra and Calculations. The calculated structural parameters of phen$^{\bullet -}$ (UB3LYP/6-311+G(d,p)) and [Cu(phen$^{\bullet -}$)$(PH_3)_2$] (UB3LYP/6-31G(d)) are shown in Table 1. The changes in bond lengths upon the reduction of phen lie between −0.06 and 0.04 Å and between −0.03 and 0.04 Å for the reduction of the Cu(I) complex. The most significant structural changes that occur upon the reduction of phen occur in bonds: N1−C12, C3−C4, C11−C12, and C13−14 with changes of 0.03−0.06 Å.

Using the optimized geometry of phen$^{\bullet -}$, we calculated the vibrational frequencies of phen$^{\bullet -}$ and d_8-phen$^{\bullet -}$. These are shown in Table 3, along with previously reported RR bands of Li^+phen$^{\bullet -}$.[10,11]

In the 1000−1700 cm^{-1} region of the RR spectra, 16 modes are observed for phen$^{\bullet -}$.[10,11] The majority of these modes are expected to have a_1 symmetry because these are the bands that will exhibit resonance enhancement.[42] Most of the bands observed in the RR spectra of phen$^{\bullet -}$ [10,11] correlate to a_1 modes, as predicted by the calculation. The exceptions are the 1254-cm^{-1} band attributed to ν_{40}, the band at 1405 cm^{-1} (ν_{45}), and the band observed at 1421 cm^{-1} (ν_{46}), which all have b_2 symmetry. Calculated frequencies are on average within 16 cm^{-1} of the observed frequency. These discrepancies may be partially attributed to the experimental data, which appears to have an uncertainty of up to 16 cm^{-1},[43] and the possibility that some of the observed bands may be due to phen^{2-}.[44] The two strongest bands that are observed in the spectra collected by Leroi et al. are at 1043 and 1449 cm^{-1} (with a 406.8-nm excitation wavelength). These are predicted to be 1023 cm^{-1} (ν_{32}) and 1443 cm^{-1} (ν_{47}), respectively.

The chemical formation of phen$^{\bullet -}$ is difficult to achieve.[44] An alternate method of probing radical anion features is to utilize excited-state species of complexes such as $[Cu(L)(PPh_3)_2]^+$ or $[Re(L)(CO)_3Cl]$ (L = bidentate ligand) in which the excited state has an MLCT formulation.[8,9] Thus, [Cu(II)(L$^{\bullet -}$)$(PPh_3)_2]^+$ or [Re(II)(L$^{\bullet -}$)$(CO)_3$Cl] is the excited-state species formed. Collecting the TR^3 spectra of $[Cu(phen)(PPh_3)_2]^+$ and [Cu(d_8-phen)$(PPh_3)_2]^+$ allows characteristic modes due to phen$^{\bullet -}$ and d_8-phen$^{\bullet -}$, respectively, to be observed through the creation of an MLCT excited state. The TR^3 spectra and the ground-state

TABLE 3: Calculated and Experimental Vibrational Spectral Data of Phen$^{\bullet -}$ and d_8-Phen$^{\bullet -}$

		phen$^{\bullet -}$		Li^+phen$^{\bullet -}$		d_8-phen$^{\bullet -}$	
		B3LYP/6-311+G(d,p)		exptl[c]	exptl[d]	B3LYP/6-311+G(d,p)	
ν[a]		ν/cm^{-1}	(IR, R Int)[b]	ν/cm^{-1}	ν/cm^{-1}	ν/cm^{-1}	(IR, R Int)[b]
31	b_2	1012	(100, 1)			999	(87, 6)
32	a_1	1023	(0, 1)	1043		839	(0, 3)
33	a_1	1042	(2, 1)	1066		865	(1, 4)
34	b_2	1051	(9, 0)			831	(1, 0)
35	a_1	1130	(2, 10)	1130	1119	950	(0, 0)
36	b_2	1141	(11, 3)			810	(12, 2)
37	a_1	1144	(1, 3)	1177		977	(9, 6)
38	b_2	1180	(44, 0)			1007	(8, 0)
39	a_1	1216	(0, 11)	1221	1212	1103	(0, 0)
40	b_2	1243	(3, 0)		1254	1018	(100, 14)
41	a_1	1308	(10, 10)	1273	1281	1169	(0, 6)
42	a_1	1320	(0, 1)	1340	1335	1272	(0, 1)
43	a_1	1375	(1, 0)	1390		1326	(6, 0)
44	b_2	1381	(3, 0)			1239	(3, 0)
45	b_2	1390	(46, 0)	1405		1280	(32, 0)
46	b_2	1417	(66, 0)		1421	1384	(53, 0)
47	a_1	1443	(1, 5)	1449	1453	1374	(3, 9)
48	b_2	1461	(45, 0)			1390	(14, 0)
49	a_1	1463	(10, 1)	1499	1515	1433	(3, 1)
50	a_1	1546	(2, 100)	1539	1543	1519	(1, 100)
51	b_2	1558	(53, 1)	1576		1530	(40, 1)
52	a_1	1595	(0, 46)	1606	1587	1565	(1, 89)

[a] Mode numbers and symmetries are from the B3LYP/6-311+G(d,p) calculation of phen [b] IR and Raman intensities have been normalized such that the strongest band in the region of interest is given an intensity of 100. Raman intensities have been calculated using an excitation wavelength of 1064 nm. [c] Reference 10. [d] Reference 11.

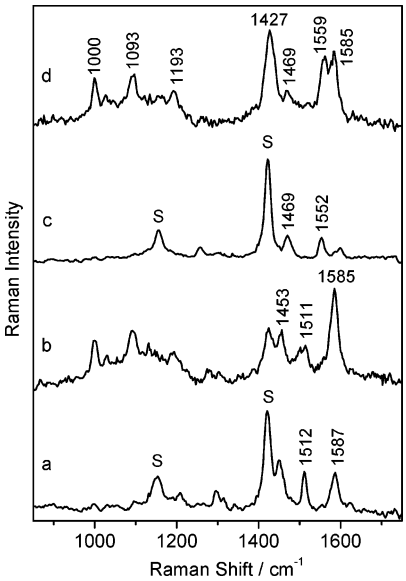

Figure 3. Resonance Raman spectra of complexes in CH_2Cl_2 (10 mmol dm^{-3}): (a) [Cu(phen)$(PPh_3)_2]^+$, λ_{exc} = 356.4 nm, 60 mW; (b) [Cu(phen)$(PPh_3)_2]^{+}$*, λ_{exc} = 354.7 nm, 2.5 mJ per pulse; (c) [Cu(d_8-phen)$(PPh_3)_2]^+$, λ_{exc} = 356.4 nm, 60 mW; (d) [Cu(d_8-phen)$(PPh_3)_2]^{+}$*, λ_{exc} = 354.7 nm, 2.5 mJ per pulse.

RR spectra of these complexes are shown in Figure 3. The spectrum of each was measured at three pulse powers to determine if mixtures of the ground and excited states were present. The excited-state lifetimes of these complexes are sufficiently long to allow an excited-state spectrum to be collected. [Cu(phen)$(PPh_3)]BF_4$ in dichloromethane has an excited-state lifetime (τ) of 220 ns at 25 °C.[45] For other phen complexes, it has been found that deuteration does not have a large effect on the excited-state lifetime.[46] Using nanosecond pulsed excitation, it is possible to probe short-lived excited states (τ < 6 ns) with high laser pulse powers.[47,48]

The similarity of the excitation wavelengths used for cw (356.4 nm) and pulsed studies (354.7 nm) makes it straightforward to identify excited-state features. Evidence of an excited state of [Cu(phen)$(PPh_3)_2]^+$, designated [Cu(phen)$(PPh_3)_2]^{+}$*, in the TR[3] spectrum comes from comparison to the ground-state RR spectra.

The spectrum of [Cu(phen)$(PPh_3)_2]^+$ with pulsed excitation and a photon/molecule ratio of 15:1[49] shows features at 999, 1029, 1092, and 1192 cm^{-1}; additional features at 1453, 1511, and 1585 cm^{-1} are also observed. The intensities of these bands do not change with increased or reduced photon flux. This means that a single state is being probed, not a mixture of ground and excited states. However, the spectrum differs significantly from the ground-state spectrum generated with 356.4-nm cw excitation. [Cu(phen)$(PPh_3)_2]^{+}$* is a better scatterer than [Cu(phen)$(PPh_3)_2]^+$ by a factor of approximately 3 at this excitation wavelength.[50] The 1295-cm^{-1} band in the ground state is absent from the spectra obtained with pulsed excitation. The spectrum shown in Figure 3 is thus attributed to [Cu(phen)$(PPh_3)_2]^{+}$*. The spectra obtained from [Cu(d_8-phen)$(PPh_3)_2]^+$ with pulsed excitation bear some similarities to that of [Cu(phen)$(PPh_3)_2]^+$ generated under the same conditions. Bands are observed at 1000, 1028, 1093, 1193, and 1585 cm^{-1}, with additional bands being present at 1469 and 1559 cm^{-1}. The spectrum with pulsed excitation is attributed to an excited-state species because the ground-state band at 1257 cm^{-1} is absent.

There are some striking similarities between the spectra of [Cu(phen)$(PPh_3)_2]^{+}$* and that of [Cu(d_8-phen)$(PPh_3)_2]^{+}$*. One possible reason for this is that the vibrational signatures of phen$^{\bullet -}$ and d_8-phen$^{\bullet -}$ are the same. This does not correlate well with our calculations that show significant shifts between the phen$^{\bullet -}$ and d_8-phen$^{\bullet -}$ species (Table 3). Another possibility is that some of the observed spectral features are due to a moiety other than phen$^{\bullet -}$ (or d_8-phen$^{\bullet -}$). To test this, the RR spectrum of $[Cu(PPh_3)_4]^+$ was measured using 354.7-nm pulsed excitation. The spectrum shows a series of bands at 1001, 1029, 1098, 1190, and 1588 cm^{-1}. These bands are observed in the RR spectra of [Cu(phen)$(PPh_3)_2]^{+}$* and [Cu(d_8-phen)$(PPh_3)_2]^{+}$* and are attributed to PPh_3. The residual bands in the spectra of the Cu complexes are then attributed to phen$^{\bullet -}$ and d_8-phen$^{\bullet -}$ species.

The phen$^{\bullet -}$ features evident in the [Cu(phen)$(PPh_3)_2]^{+}$* spectrum lie at 1453 and 1511 cm^{-1}. An additional band at 1585 cm^{-1} is also assigned as a phen$^{\bullet -}$ mode. Although it is coincident with a PPh_3 band, the band in the [Cu(phen)$(PPh_3)_2]^{+}$* spectrum is too intense to be solely caused by a PPh_3 vibration. This assignment is supported by the [Cu(d_8-phen)$(PPh_3)_2]^{+}$* data in which d_8-phen$^{\bullet -}$ modes are observed at 1469 and 1559 cm^{-1}. Significantly, the 1585-cm^{-1} PPh_3 mode is also evident, with a band intensity that is approximately half that of the 702-cm^{-1} solvent band, which is less than that in the [Cu(phen)$(PPh_3)_2]^{+}$* spectrum. One of the advantages of comparing the [Cu(phen)$(PPh_3)_2]^{+}$* and [Cu(d_8-phen)$(PPh_3)_2]^{+}$* spectra is that the electronic properties of the isotopomers are equivalent and their RR spectra may be directly compared. Thus, the PPh_3 modes in the spectrum of [Cu(d_8-phen)$(PPh_3)_2]^{+}$* possess the same intensity pattern as those in the [Cu(phen)$(PPh_3)_2]^{+}$* spectrum. Clearly, the much higher intensity of the 1585-cm^{-1} band in [Cu(phen)$(PPh_3)_2]^{+}$* cannot then be solely attributed to the PPh_3 mode. A similar procedure can be used to find an additional band in the [Cu(d_8-phen)$(PPh_3)_2]^{+}$* spectrum due to d_8-phen$^{\bullet -}$. In the spectrum of [Cu(d_8-phen)$(PPh_3)_2]^{+}$*, there is a band at 1427 cm^{-1} that is due to d_8-phen$^{\bullet -}$; this overlaps

TABLE 4: Calculated Vibrational Data of $[Cu(phen)(PH_3)_2]$ and Experimental Transient Resonance Raman Spectral Data of $[Cu(phen)(PPh_3)_2]^+$ and the Deuterated Analogues

		$[Cu(phen^{\bullet -})(PH_3)_2]$		$[Cu(phen)(PPh_3)_2]^{+*}$	$[Cu(d_8\text{-}phen^{\bullet -})(PH_3)_2]$		$[Cu(d_8\text{-}phen)(PPh_3)_2]^{+*}$
		B3LYP/6-31G(d)		exptl	B3LYP/6-31G(d)		exptl
ν[a]		ν/cm^{-1}	(IR, R Int)[b]	ν/cm^{-1}	ν/cm^{-1}	(IR, R Int)	ν/cm^{-1}
45	b_2	1001	(32, 1)		974	(35, 1)	
47	a_1	1046	(0, 0)		863	(0, 1)	
49	b_2	1065	(15, 3)		834	(3, 1)	
50	a_1	1069	(1, 1)				
52	$b_2 + PH_3$	1102	(1, 1)		1103	(1, 0)	
54	b_2	1107	(39, 5)		859	(0, 0)	
56	a_1	1137	(0, 14)		826	(0, 9)	
57	b_2	1176	(57, 15)		1160	(100, 25)	
58	a_1	1176	(0, 2)		883	(0, 4)	
59	b_2	1187	(26, 0)		1018	(2, 0)	
60	a_1	1224	(1, 19)		1122	(0, 4)	
61	b_2	1244	(0, 0)		998	(0, 0)	
62	a_1	1293	(12, 7)		1174	(1, 6)	
63	a_1	1344	(0, 13)		1293	(3, 3)	
64	b_2	1399	(21, 1)				
65	b_2	1415	(4, 2)		1257	(1, 1)	
66	a_1	1415	(2, 6)		1344	(5, 20)	
67	b_2	1453	(21, 0)		1387	(49, 4)	
68	a_1	1454	(0, 1)	1453	1426	(3, 3)	1427
69	b_2	1471	(100, 5)		1438	(99, 2)	
70	a_1	1524	(20, 2)	1511	1467	(27, 30)	1469
71	a_1	1534	(1, 100)		1514	(2, 80)	
72	b_2	1564	(1, 3)		1532	(9, 5)	
73	a_1	1602	(1, 54)	1585	1573	(1, 100)	1559

[a] Mode numbers are from the B3LYP/6-31G(d) calculation of $[Cu(phen^{\bullet -})(PH_3)_2]$. Mode symmetries are based on the C_{2v} symmetry of $phen^{\bullet -}$. Calculated modes due to PH_3 in this region have been omitted [b] IR and Raman intensities have been normalized such that the strongest band in the region of interest is given an intensity of 100. Raman intensities have been calculated using an excitation wavelength of 1064 nm.

with the solvent feature at 1423 cm^{-1}, but the increased bandwidth and frequency shift allow for its identification.

The RR spectrum of $[Os(phen)(py)_4]^{2+}$ (py = pyridine) under pulsed excitation was previously reported by Leroi et al.[10] They attribute two bands to $phen^{\bullet -}$ features at 1275 and 1580 cm^{-1}. The latter was seen at 1585 cm^{-1} in the $[Cu(phen)(PPh_3)_2]^{+*}$ spectrum. The 1275-cm^{-1} band was not seen in the $[Cu(phen)(PPh_3)_2]^{+*}$ spectrum; however, it may possibly be correlated to the 1273-cm^{-1} band that was observed in the RR spectra of $Li^+phen^{\bullet -}$, predicted as ν_{41} at 1308 cm^{-1}. Schoonover et al. report the RR spectrum of $[Ru(phen^{\bullet -})(phen)_2]^{2+*}$,[11] and in the region from 1100−1650 cm^{-1}, seven bands were assigned as being due in part or in full to $phen^{\bullet -}$ modes. Because of the closeness in frequency of $phen^{\bullet -}$ and phen modes, many of these bands overlap. There are three bands seen at 1130, 1272, and 1585 cm^{-1} assigned as $phen^{\bullet -}$ bands that are not overlapping with phen. These features are of modest intensity in comparison to that of neutral phen modes enhanced through the phen → Ru(III) ligand-to-metal charge-transfer transition.[11] The 1272- and 1585-cm^{-1} bands can be attributed to the same modes that produced the 1275- and 1580-cm^{-1} bands in the $[Os(phen)(py)_4]^{2+*}$ spectrum. The additional band at 1130 cm^{-1} is not seen in the $[Os(phen)(py)_4]^{2+*}$ or $[Cu(phen)(PPh_3)_2]^{+*}$ spectra; however, it may possibly be correlated to the 1119-cm^{-1} band of $Li^+phen^{\bullet -}$ that they also reported.[10]

For the spectra of $[Cu(phen)(PPh_3)_2]^{+*}$ and $[Cu(d_8\text{-phen})(PPh_3)_2]^{+*}$, the three bands that we have assigned as radical anion modes are at similar frequencies to the ground-state bands (within 7 cm^{-1}). This is hardly surprising considering the rigidity of phen. The addition of an electron is not likely to perturb the vibrational modes greatly.[11] The deuteration of the ligand has proved to be an important aid in identifying radical anion modes.

Previous studies have involved the identification of MLCT excited-state bands by comparison to the radical anion spectrum of the polypyridyl ligand,[9a,10,11] so it seems reasonable to assume that the calculation of the radical anion spectrum of $phen^{\bullet -}$ may aid in identifying the bands observed in the TR^3 spectrum of $[Cu(phen)(PPh_3)_2]^{+*}$. The modes observed in the TR^3 spectrum of $[Cu(phen)(PPh_3)_2]^+$ may be matched to modes observed in the RR spectra of $Li^+phen^{\bullet -}$ and thus in turn to the calculated $phen^{\bullet -}$ modes (Table 3). However, the frequencies calculated for $phen^{\bullet -}$ and those observed in the TR^3 spectrum are sufficiently different that the assignment of the bands is ambiguous. This means that using $phen^{\bullet -}$ as a model for $[Cu(phen)(PPh_3)_2]^{+*}$ is not satisfactory. This may indicate a degree of orbital mixing that makes the assumption of the transfer of a full electron from a metal-centered to ligand-based orbital invalid or that indicates that the copper center has a larger effect on the position of bands than may be anticipated. To improve the model, the $[Cu(I)(PH_3)_2]^+$ moiety has been incorporated into the calculation. In the simplified description of the MLCT excited state of $[Cu(phen)(PPh_3)_2]^+$, Cu(I) is oxidized to Cu(II) with the reduction of phen to $phen^{\bullet -}$; however, we have simply considered the reduction of $[Cu(phen)(PPh_3)_2]^+$ to $[Cu(phen^{\bullet -})(PPh_3)_2]$, which neglects the change in the oxidation state of the Cu center. Furthermore, the calculation of $[Cu(phen^{\bullet -})(PH_3)_2]$ appears to be less affected by the configuration interaction of the a_2 and b_1 molecular orbitals, the SOMO and SOMO+1, for $phen^{\bullet -}$. We note that the energy difference between the SOMO and SOMO+1 is significantly larger for $[Cu(phen^{\bullet -})(PH_3)_2]$, where the SOMO is b_1 in character, than for $phen^{\bullet -}$, therefore reducing the configuration interaction of these molecular orbitals. The $[Cu(phen^{\bullet -})(PH_3)_2]$ calculation better represents the experimental data and hence provides a better model of the excited state.

The optimized structure of $[Cu(phen^{\bullet -})(PH_3)_2]$ (B3LYP/6-31G(d)) was used to calculate vibrational frequencies and these

are compared to the TR^3 spectra of $[Cu(phen)(PPh_3)_2]^{+*}$ and $[Cu(d_8\text{-phen})(PPh_3)_2]^{+*}$ (Table 4 and Figure 3).

In the TR^3 spectrum of $[Cu(phen)(PPh_3)_2]^{+*}$, there is a band observed at 1453 cm^{-1}. This is predicted to lie at 1454 cm^{-1} (ν_{68}). Upon deuteration, this band shifts to 1427 cm^{-1}, predicted at 1426 cm^{-1}. The band observed at 1511 cm^{-1} corresponds to ν_{70}, calculated to be 1524 cm^{-1}. This indicates one of the significant differences that this improved model produces because the closest band predicted for $phen^{\bullet -}$ occurs at 1546 cm^{-1}. ν_{70} shifts to 1469 cm^{-1} upon deuteration, predicted at 1467 cm^{-1}. The band at 1585 cm^{-1} is predicted at 1602 cm^{-1} (ν_{73}). Upon deuteration, this is observed to decrease in frequency by 26 cm^{-1}, and the calculation predicts a decrease of 29 cm^{-1}.

Perhaps an even better method of modeling the TR^3 spectra would be to do a frequency calculation on the excited state. However, the frequency calculation for $[Cu(phen^{\bullet -})(PH_3)_2]$ is significantly simpler than that for $[Cu(phen)(PH_3)_2]^{+*}$ [51] and has provided a reasonable prediction of the TR^3 spectra, both of $[Cu(phen)(PPh_3)_2]^{+*}$ and its perdeuterated analogue.

Conclusions

Density functional theory, B3LYP/6-31G(d), has been successfully utilized to carry out a normal coordinate analysis of phen and its perdeuterated analogue, d_8-phen. The larger basis set 6-311+G(d,p) offers no improvement in the prediction of the vibrational spectra or structure but is necessary in order to obtain $phen^{\bullet -}$ as a $^2B_1$ state, in agreement with experimental findings, rather than the $^2A_2$ state that B3LYP/6-31G(d) predicts. The structure calculated upon reduction shows changes of less than 0.06 Å in bond length from those of neutral phen. The calculated modes have been compared to previously measured RR spectra of $phen^{\bullet -}$ and were found to be in reasonable agreement. The TR^3 spectra of $[Cu(phen)(PPh_3)_2]^+$ and $[Cu(d_8\text{-phen})(PPh_3)_2]^+$ were collected and found to have several identical bands due to the PPh_3 ligand. A consideration of the deuterated complex is necessary to aid in spectral assignment. The TR^3 spectra of $[Cu(phen)(PPh_3)_2]^+$ and $[Cu(d_8\text{-phen})(PPh_3)_2]^+$ are not well predicted by the $phen^{\bullet -}$ calculation despite it being the MLCT excited state that is being probed. However, calculations on $[Cu(phen^{\bullet -})(PH_3)_2]$ and $[Cu(d_8\text{-phen}^{\bullet -})(PH_3)_2]$ do provide a reasonable prediction.

Acknowledgment. Support from the Foundation for Research, Science & Technology, the MacDiarmid Institute for Advanced Materials and Nanotechnology, and the University of Otago is gratefully acknowledged.

References and Notes

(1) Dietrich-Buchecker, C.; Sauvage, J. P.; Kern, J. M. *J. Am. Chem. Soc.* **1989**, *111*, 7791. Armaroli, N.; Diederich, F.; Dietrich-Buchecker, C. O.; Flamigni, L.; Marconi, G.; Nierengarten, J. F.; Sauvage, J. P. *Chem.—Eur. J.* **1998**, *4*, 406. Kern, J. M.; Sauvage, J. P.; Weidmann, J. L.; Armaroli, N.; Flamigni, L.; Ceroni, P.; Balzani, V. *Inorg. Chem.*, **1997**, *36*, 5329. Chambron, J. C.; Collin, J. P.; Dalbavie, J. O.; Dietrich-Buchecker, C. O.; Heitz, V.; Odobel, F.; Solladie, N.; Sauvage, J. P. *Coord. Chem. Rev.* **1998**, *180*, 1299.

(2) Ziessel, R. *Chem. Commun.* **1988**, 16. Ziessel, R. *Angew. Chem., Int. Ed. Engl.* **1991**, *30*, 844.

(3) Tyson, D. S.; Castellana, F. N. *Inorg. Chem.* **1999**, *38*, 4382. Joshi, H. S.; Jamshidi, R.; Tor, Y. *Angew. Chem., Int. Ed.* **1999**, *38*, 2722.

(4) Crosby, G. A. *J. Chem. Educ.* **1983**, *60*, 791.

(5) Perkampus, H. H.; Rother, W. *Spectrochim. Acta, Part A* **1974**, *30*, 597.

(6) Thornton, D. A.; Watkins, G. M. *Spectrochim. Acta, Part A* **1991**, *47*, 1085.

(7) Muniz-Miranda, M. *J. Phys. Chem. A* **2000**, *104*, 7803.

(8) Kumar, C. V.; Barton, J. K.; Turro, N. J.; Gould, I. R. *Inorg. Chem.* **1987**, *26*, 1455.

(9) (a) Bradley, P. G.; Kress, N.; Hornberger, B. A.; Dallinger, R. F.; Woodruff, W. H. *J. Am. Chem. Soc.* **1981**, *103*, 7441. (b) Smothers, W. K.; Wrighton, M. S. *J. Am. Chem. Soc.* **1983**, *105*, 1067. (c) Gordon, K. C.; McGarvey, J. J. *Inorg. Chem.* **1991**, *30*, 2987.

(10) Turro, C.; Chung, Y. C.; Leventis, N.; Kuchenmeister, M. E.; Wagner, P. J.; Leroi, G. E. *Inorg. Chem.* **1996**, *35*, 5104.

(11) Schoonover, J. R.; Omberg, K. M.; Moss, J. A.; Bernhard, S.; Malueg, V. J.; Woodruff, W. H.; Meyer, T. J. *Inorg. Chem.* **1998**, *37*, 2585.

(12) Stoyanov, S. R.; Villegas, J. M.; Rillema, D. P. *Inorg. Chem.* **2002**, *41*, 2941.

(13) Zheng, K. C.; Wang, J. P.; Peng, W. L.; Shen, Y.; Yun, F. C. *Inorg. Chim. Acta* **2002**, *328*, 247. Zheng, K. C.; Wang, J. P.; Shen, Y.; Peng, W. L.; Yun, F. C. *J. Chem. Soc., Dalton Trans.* **2002**, 111. Zheng, K. C.; Wang, J. P.; Shen, Y.; Peng, W. L.; Yun, F. C. *J. Comput. Chem.* **2002**, *23*, 436−443.

(14) Diaz-Acosta, I.; Baker, J.; Cordes, W.; Pulay, P. *J. Phys. Chem. A* **2001**, *105*, 238.

(15) Matthewson, B. J.; Flood, A.; Polson, M. I. J.; Armstrong, C.; Phillips, D. L.; Gordon, K. C. *Bull. Chem. Soc. Jpn.* **2002**, *75*, 933.

(16) Stoyanov, S. R.; Villegas, J. M.; Rillema, D. P. *Inorg. Chem.* **2002**, *41*, 2941.

(17) Dattelbaum, D. M.; Omberg, K. M.; Schoonover, J. R.; Martin, R. L.; Meyer, T. J. *Inorg. Chem.* **2002**, *41*, 6071.

(18) Ould-Moussa, L.; Poizat, O.; Castella-Ventura, M.; Buntinx, G.; Kassab, E. *J. Phys. Chem.* **1996**, *100*, 2072.

(19) Damrauer, N. H.; Weldon, B. T.; McCusker, J. K. *J. Phys. Chem. A* **1998**, *102*, 3382.

(20) Kaim, W. *J. Am. Chem. Soc.* **1982**, *104*, 3833.

(21) Klein, A.; Kaim, W.; Waldhoer, E.; Hausen, H.-D. *J. Chem. Soc., Perkin Trans. 2* **1995**, 2121.

(22) Ernst, S.; Vogler, C.; Klein, A.; Kaim, W. *Inorg. Chem.* **1996**, *35*, 1295.

(23) Junk, T.; Catallo, W. J.; Elguero, J. *Tetrahedron Lett.* **1997**, *38*, 6309.

(24) Rader, R. A.; McMillin, D. R.; Buckner, M. T.; Matthews, T. G.; Casadonte, D. J.; Lengel, R. K.; Whittaker, S. B.; Darmon, L. M.; Lytle, F. E. *J. Am. Chem. Soc.* **1981**, *103*, 5906.

(25) Microanalyses were obtained using a Carlo Erba EA1108 with TCD detection for H_2O or D_2O.

(26) Shriver, D. B.; Dunn, B. R. *Appl. Spectrosc.* **1974**, *28*, 319.

(27) McCreery, R. L. *Raman Spectroscopy for Chemical Analysis*; Winefordner, J., Ed.; Wiley Chemical Analysis Series; Wiley & Sons: New York, 2000; Vol. 157.

(28) The ASTM subcommittee on Raman spectroscopy has adopted eight materials as Raman shift standards (ASTM E 1840). The band wavenumbers for these standards are available at http://chemistry.ohio-state.edu/~rmccreer/shift.html.

(29) Frisch, M. J.; Trucks, G. W.; Schlegel, H. B.; Scuseria, G. E.; Robb, M. A.; Cheeseman, J. R.; Zakrzewski, V. G.; Montgomery, J. A., Jr.; Stratmann, R. E.; Burant, J. C.; Dapprich, S.; Millam, J. M.; Daniels, A. D.; Kudin, K. N.; Strain, M. C.; Farkas, O.; Tomasi, J.; Barone, V.; Cossi, M.; Cammi, R.; Mennucci, B.; Pomelli, C.; Adamo, C.; Clifford, S.; Ochterski, J.; Petersson, G. A.; Ayala, P. Y.; Cui, Q.; Morokuma, K.; Malick, D. K.; Rabuck, A. D.; Raghavachari, K.; Foresman, J. B.; Cioslowski, J.; Ortiz, J. V.; Stefanov, B. B.; Liu, G.; Liashenko, A.; Piskorz, P.; Komaromi, I.; Gomperts, R.; Martin, R. L.; Fox, D. J.; Keith, T.; Al-Laham, M. A.; Peng, C. Y.; Nanayakkara, A.; Gonzalez, C.; Challacombe, M.; Gill, P. M. W.; Johnson, B. G.; Chen, W.; Wong, M. W.; Andres, J. L.; Head-Gordon, M.; Replogle, E. S.; Pople, J. A. *Gaussian 98*, revision A.7; Gaussian, Inc.: Pittsburgh, PA, 1998.

(30) Frisch, M. J.; Trucks, G. W.; Schlegel, H. B.; Scuseria, G. E.; Robb, M. A.; Cheeseman, J. R.; Montgomery, J. A., Jr.; Vreven, T.; Kudin, K. N.; Burant, J. C.; Millam, J. M.; Iyengar, S. S.; Tomasi, J.; Barone, V.; Mennucci, B.; Cossi, M.; Scalmani, G.; Rega, N.; Petersson, G. A.; Nakatsuji, H.; Hada, M.; Ehara, M.; Toyota, K.; Fukuda, R.; Hasegawa, J.; Ishida, M.; Nakajima, T.; Honda, Y.; Kitao, O.; Nakai, H.; Klene, M.; Li, X.; Knox, J. E.; Hratchian, H. P.; Cross, J. B.; Adamo, C.; Jaramillo, J.; Gomperts, R.; Stratmann, R. E.; Yazyev, O.; Austin, A. J.; Cammi, R.; Pomelli, C.; Ochterski, J. W.; Ayala, P. Y.; Morokuma, K.; Voth, G. A.; Salvador, P.; Dannenberg, J. J.; Zakrzewski, V. G.; Dapprich, S.; Daniels, A. D.; Strain, M. C.; Farkas, O.; Malick, D. K.; Rabuck, A. D.; Raghavachari, K.; Foresman, J. B.; Ortiz, J. V.; Cui, Q.; Baboul, A. G.; Clifford, S.; Cioslowski, J.; Stefanov, B. B.; Liu, G.; Liashenko, A.; Piskorz, P.; Komaromi, I.; Martin, R. L.; Fox, D. J.; Keith, T.; Al-Laham, M. A.; Peng, C. Y.; Nanayakkara, A.; Challacombe, M.; Gill, P. M. W.; Johnson, B.; Chen, W.; Wong, M. W.; Gonzalez, C.; Pople, J. A.; *Gaussian 03* Gaussian, Inc.: Pittsburgh, PA, 2003.

(31) Schaftenaar, G.; Noordik, J. H. *J. Comput.-Aided Mol. Des.* **2000**, *14*, 123.

(32) Drew, M G. B.; Bin Othman, A. H.; McFall, S. G.; Nelson, S. M. *J. Chem. Soc., Chem. Commun.* **1977**, 558.

(33) Kirchhoff, J. R.; McMillin, D. R.; Robinson, W. R.; Powell, D. R. *Inorg. Chem.* **1985**, 24, 2928.

(34) Martínez, A.; Salcedo, R.; Sansores, L. E. *Inorg. Chem*. **2001**, *40*, 301.

(35) Guirgis, G. A.; Nashed, Y. E.; Durig, J. R. *Spectrochim. Acta, Part A* **2000**, *56*, 1065.

(36) The scale factors were calculated from a root-mean-square analysis of the calculated and observed modes of phen in the region from 1000−1700 cm^{-1}. In the case of phen, only modes that are at least 10% of the intensity of the strongest band observed in this region are considered. This is not done for $[Cu(phen)(PPh_3)_2]^+$ because the intensity of the bands is affected by PPh_3 modes.

(37) Foresman, J. B.; Frisch, *Æ. Exploring Chemistry with Electronic Structure Methods*, 2nd ed.; Gaussian, Inc.: Pittsburgh, PA, 1996.

(38) (a) Nakamoto, K. *Infrared and Raman Spectra of Inorganic and Coordination Compounds, Part A: Theory and Applications in Inorganic Chemistry*, 5th ed.; Wiley & Sons: New York, 1997. (b) Balakrishnan, G.; Mohandas, P.; Umapathy, S. *Spectrochim. Acta, Part A* **1997**, *53*, 1553.

(39) Grafton, A. K.; Wheeler, R. A. *Comput. Phys. Commun.* **1998**, *113*, 78.

(40) Thornton, D. A.; Watkin, G. M. *J. Coord. Chem*. **1992**, *25*, 299.

(41) Campos-Vallette, M. M.; Clavijo, R. E.; Mendizabel, F.; Zamudio, W.; Baraona, R.; Diaz, G. *Vib. Spectrosc*. **1996**, *12*, 37.

(42) Clarke, R. J. H.; Dines, T. J. *Angew. Chem., Int. Ed. Engl.* **1986**, *25*, 131.

(43) The data in Table 1 of the paper by Leroi et al.[10] show uncertainties in the band positions reported. An example of this is the 1490-cm^{-1} band, measured with excitation wavelengths of 568 and 647 nm, which appears at 1506 cm^{-1} with 406.8-nm excitation and at 1499 cm^{-1} with 351.1- and 363.8-nm excitation. This uncertainty has probably resulted from problems with calibration files. Comparison with the $Li^+phen^{\bullet -}$ bands reported by Schoonover et al.[11] also shows discrepancies in the wavenumbers of bands.

(44) Maleug, V. J. M. A. Thesis, University of Texas at Austin, Austin, TX, 1981.

(45) Palmer, C. E. A.; McMillin, D. R. *Inorg. Chem*. **1987**, *26*, 3837.

(46) Meyer, T. J. In *Progress in Inorganic Chemistry;* Lippard, S. J., Ed.; Wiley & Sons: New York, 1983; Vol. 30. Kober, E. M.; Marshall, J. L.; Dressick, W. J.; Sullivan, B. P.; Caspar, J. V.; Meyer, T. J. *Inorg. Chem*. **1985**, *24*, 2755.

(47) Caswell, D. S.; Spiro, T. G. *Inorg. Chem.* **1987**, *26*, 18.

(48) Gordon, K. C.; McGarvey, J. J. *Chem. Phys. Lett*. **1989**, *162*, 117.

(49) With a 1-mm penetration of the sample and a 300-μm spot size, a 10 mM solution contains 4×10^{14} molecules. A 3.6-mJ pulse of 355-nm light contains 6×10^{15} photons. The lifetimes of the complex in CH_2Cl_2 are >50 ns, and thus the relaxation within the pulse duration is negligible. The photon/molecule ratio suggests a complete conversion of the irradiated volume to the excited state.

(50) On the basis of comparisons of the ratio of the 1511/1510-cm^{-1} bands of $[Cu(phen)(PPh_3)_2]^{+*}$ and $[Cu(phen)(PPh_3)_2]^+$, respectively, to the 702-cm^{-1} solvent band.

(51) Time-dependent density functional theory calculations, implemented with the programs we have used, are unable to use analytic gradients.[30]